01 Sep 2008

Photorefractivity in a Polymeric Composite Photosensitized with NiS Nanocrystals

Tyler M. Fears

Charles Anderson

Jeffrey G. Winiarz
Missouri University of Science and Technology, winiarzj@mst.edu

Photorefractivity in a polymeric composite photosensitized with NiS nanocrystals

Tyler M. Fears, Charles Anderson, and Jeffrey G. Winiarz[a)]
Nanophotonic Materials Research Group, Missouri University of Science and Technology, Rolla, Missouri 65409, USA

(Received 7 March 2008; accepted 9 September 2008; published online 16 October 2008)

The photorefractive performance of a polymeric composite photosensitized through the inclusion of NiS nanocrystals is described. The nanocrystals were characterized using visible-absorption spectroscopy, energy-dispersive x-ray spectroscopy, and transmission electron microscopy. We further demonstrate the ability to enhance various aspects of the composite's photorefractive performance by performing ligand exchange on the nanocrystals prior to their incorporation into the polymer composite. This procedure resulted in a lowering of the overmodulation voltage from ~70 to ~50 V/μm without affecting the maximum diffraction efficiency of ~40%. An increase in the two-beam-coupling gain coefficient was similarly observed, increasing from 38 to 79 cm^{-1}. The photoconductivities were used in determining the overall quantum efficiencies associated with the photorefractive devices. All experiments were conducted at 633 nm and the data represent a significant improvement in the photorefractive performance of inorganic-organic hybrid photorefractive materials. © *2008 American Institute of Physics*. [DOI: 10.1063/1.2993253]

I. INTRODUCTION

Owing to their substantial optical nonlinearities, low permittivity, and low cost, polymeric photorefractive (PR) materials are useful in a variety of real-time optical information processing applications including beam clean-up and amplification, dynamic interferometry, phase conjugation, and pattern recognition.[1–5] Consequently, a great deal of research has focused on the development of this class of materials, resulting in significant advances, including millisecond response times and nearly 100% diffraction efficiencies.[3] Polymer based PR composites are also attractive due to the ease with which their constituents may be independently modified, allowing the eventual composite to be tailored for a specific application.

With the establishment of nanotechnology it is now possible to photosensitize PR and photoconductive polymer composites by doping them with semiconductor nanocrystals, also known as *quantum dots* or *Q-dots*,[6–18] This approach has numerous advantages, perhaps the most appealing is the ability to manipulate the spectral features of *Q*-dots, and therefore the operational wavelength of the composite into which they are doped.[6–9] Control over the optical and electrical properties of the nanocrystalline material stems from the inverse correlation between the optical band gap E_g and the physical dimension of the nanocrystal. This relationship translates into a blueshift in the absorption spectrum of a given material as its proportions are decreased beyond the dimensions of the associated Bohr radius. In addition, nanocrystals are considerably smaller than the wavelengths associated with visible light rendering the PR composite optically transparent.

While this new class of inorganic-organic hybrid polymeric composites shows enormous promise, the technology is still in its infancy. Diffraction efficiencies, operational voltages, and response times associated with PR inorganic-organic composites do not equal that of their all-organic counterparts and must be improved to meet the requirements of projected applications. In order to attend to these concerns, the fundamental mechanisms involved in photocharge generation and charge transport must be elucidated and innovative methods devised allowing for the PR performance to be optimized for a specified application. This optimization can be accomplished through variation in the constituents' stoichiometric ratio and prudent choice of the nanocrystalline photosensitizer's properties. Recently, advancements in the syntheses of semiconductor nanocrystals have significantly improved control over nanocrystal morphology, surface characteristics, and, most notably, composition. Nevertheless, with few exceptions,[10,13,14] studies concerning the photosensitization of PR polymeric composites with *Q*-dots have focused on one of four semiconductor materials: CdSe, CdS, PbSe, and PbS.

The use of heavy metals such as Pb and Cd, however, carries obvious implications with regard to the environment. Furthermore, recent regulatory pressure to decrease or eradicate the use of cadmium has added to the urgency for finding alternative materials. Primarily for this reason, we have investigated the use of more environmentally friendly materials for use as photosensitizers in photonic devices. In this communication we describe the PR performance of a series of polymeric composites photosensitized through the inclusion of NiS nanocrystals, deemed a suitable candidate due to the E_g associated with the bulk material of 0.04 eV.[19] The NiS nanocrystals were synthesized using an approach based on a previous report in the literature.[20] The nanoparticles were characterized by means of visible-absorption spectros-

[a)]Electronic mail: winiarzj@mst.edu.

copy, energy-dispersive x-ray spectroscopy (EDS), and transmission electron microscopy (TEM). In addition to producing a high-performance PR composite, we demonstrate the ability to lower the overmodulation voltage and enhance the two-beam-coupling (TBC) operation of the composite through variation in the nanocrystal's passivating molecule. In this case the passivating molecule coupled with the synthesis, oleic acid (OA), was exchanged for pyridine. The composites also contain the well characterized hole-transporting polymer, poly(*N*-vinylcarbazole) (PVK). The glass transition temperature of the composites was lowered to below ambient temperature through the inclusion of *N*-ethylcarbazole (ECZ) and the electro-optic activity was imparted through the addition of 4-homopiperidinobenzylidenemalononitrile (7-DCST).[21,22]

To characterize the performance of the composites, degenerate four-wave mixing (DFWM), asymmetric TBC, visible-absorption spectroscopy, and conductivity experiments were employed, the results and implications of which will be presented. In addition to the insights gained into the fundamental mechanisms relevant to this class of materials, the data presented represent a significant improvement over previously reported performances associated with nanocrystal-photosensitized PR composites.

II. EXPERIMENTAL

A. Synthesis of the NiS nanocrystals

All chemicals were obtained from Aldrich and used as received unless otherwise noted. NiS nanocrystals were synthesized via an adaptation of a procedure found in the literature and all manipulations were conducted using standard airless techniques.[20] Briefly, in a three-neck flask, 0.48 g of $NiCl_2 \cdot 6H_2O$ were dissolved in 18 ml of oleylamine, to which was added 0.30 ml of OA, 2.7 ml of trioctylphosphine, and 0.13 g sulfur flowers. Under mechanical stirring, the solution was degassed at 100 °C for approximately 1 h and then heated to 200 °C under nitrogen. After 90 min the black solution was removed from heat, allowed to cool to room temperature, and followed by the addition of ~10 ml of methanol. The precipitated nanocrystals were collected by centrifugation and subsequently dispersed in toluene. Several successive precipitation and dispersion cycles were conducted to remove any unreacted constituents. The product was finally dispersed in toluene and filtered to remove large aggregates and other contaminants. Half of the dispersion was then set aside for ligand exchange.

In order to conduct the ligand exchange process on the NiS nanocrystals, the OA capped nanocrystals dispersed in toluene were precipitated through the addition of methanol and centrifuged. The supernatant was discarded and the wet nanocrystals were dispersed in 10 ml of pyridine. This solution was mechanically stirred until it became optically clear (approximately 24 h). At this time the nanocrystals were precipitated through the addition of 25 ml of heptane, collected, and redispersed in pyridine. This solution was then filtered to remove any undissolved solids. Herein, the OA passivated NiS nanocrystals will be referred to as NiS:OA and those passivated with pyridine will be referred to as NiS:PY.

TABLE I. Compositions and absorptions of the PR devices used in this study.

Device	PVK (wt %)	7-DCST (wt %)	ECZ (wt %)	NiS Q-dots (wt %)	Abs., α, at $\lambda=633$ nm (cm^{-1})
OA35	49.7	34.8	14.9	0.56	34.5
OA70	49.4	34.6	14.8	1.1	69.4
OA99	49.2	34.4	14.8	1.6	98.8
PY35	49.8	34.8	14.9	0.43	35.8
PY70	49.6	34.7	14.9	0.86	67.2
PY99	49.4	34.6	14.8	1.2	96.1

The NiS nanocrystals were characterized by TEM using a Philips EM430T scanning TEM and employing carbon-coated grids. Elemental analysis was conducted using a Noran Voyager III light element EDS system. All visible-absorption spectra were recorded on a Beckman DU 640B spectrophotometer. The absorption spectra of the NiS nanoparticle suspensions were obtained using a 1 mm quartz cell at concentrations of 0.49 mg/ml in toluene for NiS:OA and 0.43 mg/ml in pyridine for NiS:PY

B. Fabrication of the PR devices

7-DCST was synthesized in our laboratory based on procedures described in the literature.[21,22] For the composite samples, PVK (secondary standard), ECZ, 7-DCST, and the appropriate type and quantity of capped NiS nanocrystals were dissolved in toluene:teterahydrofuran (13:1 by weight) and, after thorough mixing, filtered to remove any undissolved solids. This solution was stored in a vacuum oven at 50 °C for 24 h to remove the solvent. The solid residue was subsequently recovered, placed between two pieces of glass coated with indium tin oxide, and heated above its melting temperature on a hot plate. The sample was then mechanically pressed forming the typical "sandwich" geometry using glass spacers to control the thickness d of the device at 100 μm.

A total of six devices were fabricated, three for each type of NiS nanocrystal; NiS:OA and NiS:PY. Within each series of devices, the concentration of NiS was varied with the intention of achieving three particular device absorption coefficients at $\lambda=633$ nm, specifically $\alpha \approx 35$, 70, and 99 cm^{-1}. For this reason, the three PR devices photosensitized with NiS:OA will herein be referred to as OA35, OA70, and OA99. Similarly, the series of three PR devices photosensitized with NiS:PY will be referred to as PY35, PY70, and PY99. The composition of each device as well as its experimentally measured absorption coefficient at $\lambda=633$ nm is presented in Table I. For all devices, the PVK:7-DCST:ECZ ratio was held constant. To determine the weight percentage of NiS in each composite, several NiS:solvent solutions of known absorbance and volume were evaporated to dryness and the mass of the solid residue was measured. This allowed us to correlate the absorbance and concentration in g/ml of the NiS suspensions used in the device fabrication. The weight percent of NiS in each device was thus calculated indirectly from the known absorbance and volume of the

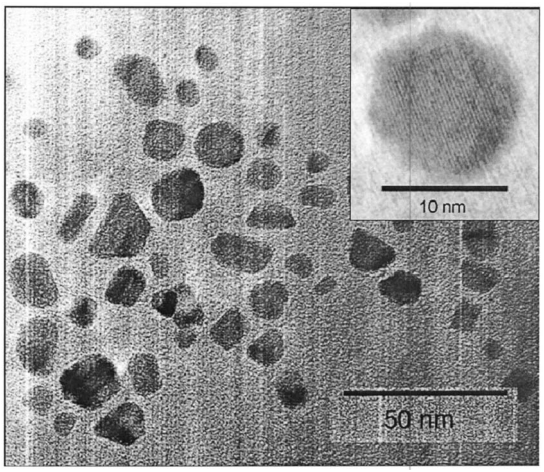

FIG. 1. TEM image of NiS:OA.

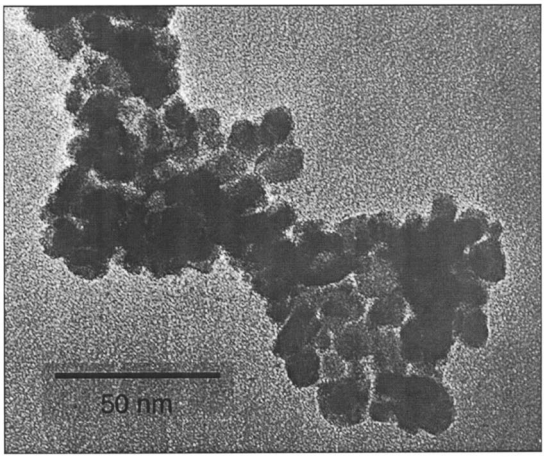

FIG. 2. TEM image of NiS:PY.

aliquot used in the fabrication of the respective composite. The PR devices have not shown any degradation of their optical properties over the course of 16 months.

C. PR characterizations

The PR properties of the composite devices were studied via TBC and DFWM techniques using a standard tilted geometry. Holographic gratings were written through the intersection of two coherent beams generated by a helium-neon (HeNe) laser operating at $\lambda=633$ nm with incident angles of $\theta_1=45°$ and $\theta_2=75°$ (in air) relative to the sample normal. In the TBC experiments, both writing beams were *p*-polarized with intensities of $I_1\approx 0.04$ mW and $I_2\approx 6$ mW. The external bias was applied such that I_1 would experience gain at the expense of I_2. Asymmetric energy transfer was observed by monitoring the intensities of the writing beams after the PR device with a photodiode. In the DFWM experiment the writing beams were *s*-polarized with intensities of $I_1\approx 3$ mW and $I_2\approx 7$ mW. In addition, a *p*-polarized probe beam with $\lambda=633$ nm propagated in a direction opposite to I_1 with an intensity of $I_p\approx 1\times 10^{-2}$ mW. Through the use of a polarizing beam splitter placed in the path of I_2 in conjunction with a photodiode, the diffracted portion of I_p, also referred to as the signal beam I_s, could be quantified. In all PR experiments, I_1 and I_2 had beam diameters of ~ 280 μm, while I_p possessed a beam diameter of ~ 120 μm. Beam diameters were measured by using a fractional irradiance of $1/e^2$.

Photoconductivity σ_p characterizations were made using a dc-photocurrent technique with a Keithley electrometer used to measure the current passing through the sample as a function of applied bias. The beam intensity for all σ_p characterizations was ~ 11 mW with a beam diameter of 0.98 mm at $\lambda=633$ nm.

III. RESULTS AND DISCUSSION

The NiS nanocrystals utilized in this study were synthesized based on a procedure found in the literature.[20] Furthermore, ligand exchange was performed on the nanocrystals, replacing OA, the passivating ligand imparted to the surface of the NiS nanocrystals during the original synthesis, for pyridine. In previous studies, this procedure has been conducted in order to improve the solubility of the nanocrystals within the polymer matrix;[18] however, on this occasion the optical quality of the final PR composites, as determined by light-scattering experiments, was found to be excellent, independent of the passivating ligands used in this study. In the current study we demonstrate that the ligand exchange process results in an improvement in the PR performance of the hybrid nanocomposite. It was initially speculated that this enhancement in the PR performance stemmed from a more efficient charge-transfer process from the nanocrystal to the charge-transporting polymer matrix. This assumption was based on the belief that the aliphatic OA would be relatively insulative with respect to the charge-transfer process, consequently impeding its efficiency. Therefore, by replacing the OA with pyridine, which due to its conjugated nature was expected to be more conducive with respect to charge transfer, we expected an increase in the efficiency of the charge-transfer process which would result in an increase in the observed σ_p, and ultimately an enhancement in the PR performance. While the ligand exchange process did result in an improvement of the composite's PR performance, experimental results indicate that this increase in the PR performance is due to a change in the trapping characteristics of the nanocrystal as a result of this surface modification. Support for this conclusion will emerge from an analysis of the data. Previous studies have demonstrated the ability of semiconductor nanocrystals to simultaneously act as both a charge-generating species as well as a charge-trapping species.[23] The charge-trapping takes place where dangling bonds and other surface defects occur and can result in an increase in the number of ways in which charge recombination may occur. This charge recombination ultimately reduces the density of free charges which can contribute to the space-charge field and reduces the PR performance of the composite.

Given the dependence of a nanocrystal's optical properties upon its size, an accurate portrayal of the latter is crucial for this study. Toward these ends, TEM was employed and the images obtained for NiS:OA and NiS:PY are presented in Figs. 1 and 2, respectively. Evident in the inset of Fig. 1 is

the lattice spacing of the NiS nanocrystal, corroborating the single crystal–domain character of the NiS nanoparticles. The particles are irregularly shaped, but generally rectangular or oblong in character. For the case of NiS:OA, the mean length was determined to be 13 ± 4.2 nm and the mean width was determined as 10 ± 2.5 nm ($N=49$). Similarly, for the NiS:PY, the mean length was calculated to be 11 ± 3.4 nm and the mean width 8.5 ± 2.6 nm ($N=18$). The relatively large standard deviations are reflective of the polydispersity associated with the nanocrystals. The data also suggest a slight reduction in the average size of the nanoparticles as a result of the pyridine treatment. This speculation was bolstered by storing NiS nanoparticles in pyridine for approximately 6 months, at the end of which time it was observed that the nanoparticles had completely dissolved into solution. Also evident in comparing Figs. 1 and 2 is that NiS:PY shows a much greater tendency for aggregation on the TEM grid. As such, achieving an accurate interpretation of the size distribution associated with the NiS:OA was uncomplicated, however, in the case of NiS:PY, only particles which could be clearly distinguished were included in the size analysis. Hence, if one sized particle has a higher propensity for aggregation over another, it is conceivable that the data obtained for NiS:PY may be skewed accordingly. It is also noted that although the NiS:PY exhibited a tendency for aggregation on the TEM grid, it was ascertained that this was not the case within the composite matrix based on the high optical quality of the PR devices as determined through light-scattering experiments.

Elemental analysis was performed on the NiS:OA and NiS:PY nanocrystals using EDS. For NiS:OA, the results revealed a Ni:(S) ratio of $1.0:(0.70 \pm 0.06)$. Here, it is assumed that excess Ni is present in order to compensate for the anionic nature of the OA passivating ligand. As expected, when the OAs were exchanged for pyridine, the excess Ni was significantly reduced, with an ensuing Ni:(S) ratio of $1.0:(0.88 \pm 0.07)$. In this case, the neutrally charged pyridine molecules do not need to be compensated by the positive charge associated with additional Ni atoms. It is expected that the superfluous Ni atoms, as well as the detached OA molecules, are removed with the washing procedure following the ligand exchange process.

Visible-absorption spectroscopy was performed on the NiS:OA and NiS:PY in solution and are presented in Fig. 3. Both spectra are normalized to 1 mg/ml. Looking initially at the spectra for NiS:OA, there exists a peak at 448 nm, and can be attributed to the first excitonic absorption. Given the polydisperse nature of the NiS:OA, as revealed by TEM, the presence of this clearly defined peak was unexpected. Equally remarkable was the drastic change in the appearance of the spectrum resulting from exchange of passivating ligands. Both pyridine and OA are transparent in the visible and as such, only a small blueshift was expected as a consequence of the slight decrease in size of the NiS nanocrystals resulting from the ligand exchange process. Indeed there does appear to be a blueshift, with a shoulder appearing at ~321 nm, but there is also the emergence of a new shoulder at ~679 nm. This may be explained as a preferential sizing resulting from the etching known to take place during the ligand exchange process, but due to the aggregation of the NiS:PY on the TEM grid, this speculation could not be confirmed with a reasonable degree of certainty. That being said, a size histogram constructed for the NiS:PY did appear to have two groupings in the lengths, with one grouping at ~7 nm and another at ~13 nm and may explain the presence of these two shoulders. The biphasic grouping is not observed in the histogram for NiS:OA. Also apparent in Fig. 3 is the fact that the area under the curve has increased for NiS:PY relative to that of NiS:OA, despite that both spectra are normalized to 1 mg/ml. This is likely due to agglomeration of the NiS:PY nanocrystals, resulting in a increase in the degree of scattering.

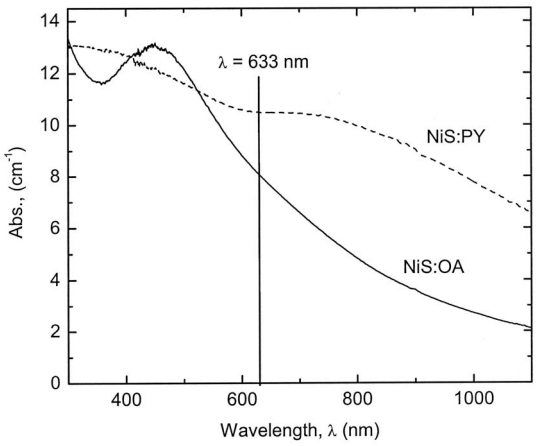

FIG. 3. Visible-absorption spectra of NiS:OA (solid line) in toluene and NiS:PY (dashed line) in pyridine.

As cited earlier, the E_g of NiS in the bulk is 0.40 eV.[19] The absorption spectrum for NiS:OA illustrates that as a result of quantization, E_g has been tailored to ~2.77 eV, therefore enlarged relative to the bulk by ~2.37 eV. The conduction band of bulk NiS lies ~5.23 eV below the vacuum level. Such a value implies that the oxidation by photoexcited bulk NiS would be energetically unfavorable given that the conduction band for PVK is known to lie 5.9 eV below the vacuum level. However, if one assumes that the widening of E_g as a consequence of quantization equally modifies the absolute positions of the valence and conduction bands by equal amounts (i.e., 2.37/2 eV), then the conduction band in NiS:OA will be positioned ~6.4 eV below the vacuum level. Therefore the oxidation of the PVK molecule by the photoexcited NiS:OA will be energetically favorable. This assumption is qualitatively confirmed through the observed photoconductivity in the PR devices used in this study. A similar argument applies to the NiS:PY/PVK system.

PR devices were fabricated using NiS nanocrystals as the photosensitizer. The concentration of NiS nanocrystals used in each device was chosen in order to achieve a predetermined absorption cross section at $\lambda = 633$ nm, α_{633}. Specifically we intended to fabricate two series of devices, one series photosensitized through the inclusion of NiS:OA and the second through the inclusion of NiS:PY, with each series composed of three devices of various NiS concentrations, selected such that $\alpha_{633} = 35$, 70, and 99 cm^{-1}. These α_{633} were preferred because they are representative of absorption

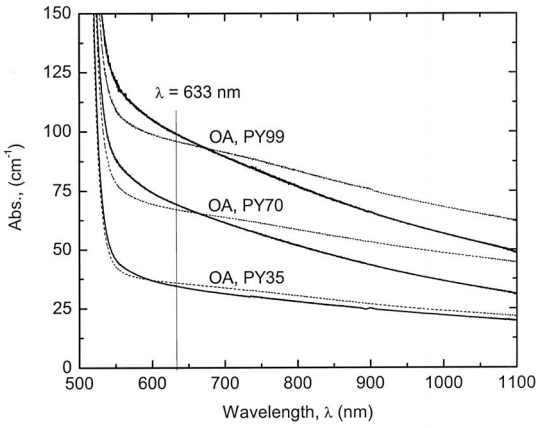

FIG. 4. Visible-absorption spectra of the NiS:OA (solid lines) and NiS:PY (dashed lines) photosensitized PR devices used in this investigation.

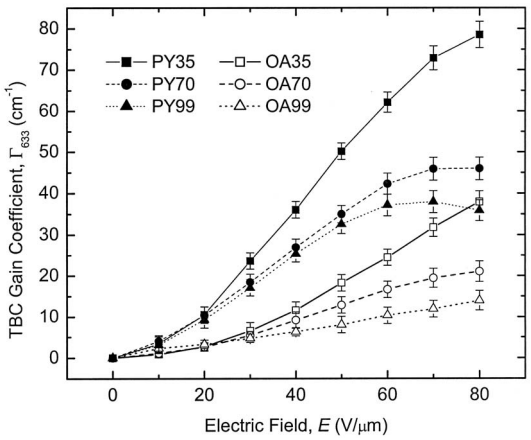

FIG. 5. Electric field dependence of the TBC gain coefficient Γ for the PR devices used in this study. The lines are guides for the eye.

cross sections of all-organic PR devices common in the literature. The actual α_{633} achieved for each device is given in Table I. Apparent from the table, for the devices photosensitized using NiS:OA, it was necessary to increase the weight percentage of photosensitizer relative to the devices photosensitized with NiS:PY in order to achieve a similar α_{633}. As explained earlier, this is attributed to the more massive capping ligands, in conjunction with the extra Ni required for charge compensation. The absorption spectra obtained for OA35, OA70, OA99, PY35, PY70, and PY99 are presented in Fig. 4.

A distinct characteristic feature of the PR effect is that the refractive index grating created in the medium is spatially shifted with respect to the light intensity pattern of the writing beams.[24] As a result, an asymmetric exchange of energy occurs between beams interfering in a PR medium. The PR nature of the gratings created within the composites used in this study was confirmed using conventional TBC experiments. The TBC gain coefficient Γ is given in terms of the experimentally measured quantities γ_0 and β as

$$\Gamma = \frac{1}{L}[\ln(\gamma_0\beta) - \ln(\beta + 1 - \gamma_0)], \tag{1}$$

where L is the path length of the beam experiencing gain inside the sample, β is the ratio of the writing beam intensities before the sample, and γ_0 is the ratio of the intensities of the beam experiencing gain with and without the pump beam. The TBC gain coefficients at $\lambda = 633$ nm, Γ_{633}, as a function of E are presented in Fig. 5 for OA35, OA70, and OA99. An examination of the data shows that as the concentration of the NiS:OA photosensitizer is increased, the TBC performance of the composite decreases. This behavior is particularly adverse since, for practical applications, the optical amplification Γ should exceed the absorption α for a given device. Therefore, OA35 with $\Gamma_{633} - \alpha_{633} = 3.4$ cm^{-1} at 80 V/μm is the only NiS:OA photosensitized device for which Γ exceeds α at any applied voltage. The OA70 device reaches a maximum of $\Gamma_{633} = 21$ cm^{-1}, which is reasonably large when compared with similar composites, but with $\alpha_{633} \approx 70$ cm^{-1}, is of little applied value.

By exchanging the OA ligands for that of pyridine, a substantial increase in the TBC efficiency was observed as illustrated in Fig. 5, which depicts the TBC data obtained for PY35, PY70, and PY99. In comparing the data obtained for the NiS:PY and NiS:OA photosensitized devices, we see that the maximum TBC gain associated with PY35 ($\Gamma_{633} = 79$ cm^{-1}) is approximately twice that measured for OA35 ($\Gamma_{633} = 38$ cm^{-1}) at 80 V/μm. This increase in Γ_{633}, as a result of ligand exchange, devoid of an increase in α_{633}, translates in to substantial increase in the figure of merit $\Gamma_{633} - \alpha_{633} = 43$ cm^{-1} at 80 V/μm. For the PY70 and PY99 devices, however, net optical gain was not observed ($\Gamma - \alpha < 0$). As with the NiS:OA photosensitized devices, for the NiS:PY photosensitized devices, an increase in the concentration of the NiS photosensitizer resulted in a decrease in the TBC performance. This behavior, observed in both series of devices, is unexpected since an increase in charge-generating species, with no appreciable change in the concentration of the other constituents, should result in an increase in the number of generated free charge carriers. This increase in free-charge carriers should translate into an increase in the photoconductivity and ultimately into an enhancement in the PR performance. Deviation from this model implies that the nanocrystalline photosensitizer is affecting the PR performance in unanticipated ways. Forthcoming analysis will lend credence to the hypothesis that the nanocrystals are also acting as trapping species with this effect being more significant in NiS:OA photosensitized devices than in NiS:PY sensitized devices. It is also noted that device void of photosensitizing NiS nanocrystals did not exhibit any PR response.

The internal diffraction efficiencies η_{int} were measured experimentally and determined according to the equation

$$\eta_{\text{int}} = \frac{I_s}{I_{p'}}, \tag{2}$$

where $I_{p'}$ is the intensity of the probe beam after the device with no bias applied and I_s is the intensity of the diffracted portion of I_p. These data are presented in Fig. 6 for OA35, OA70, and OA99. While all three devices show an overmodulation E of ~70 Vμm, a maximum η_{int} of 38.3% is

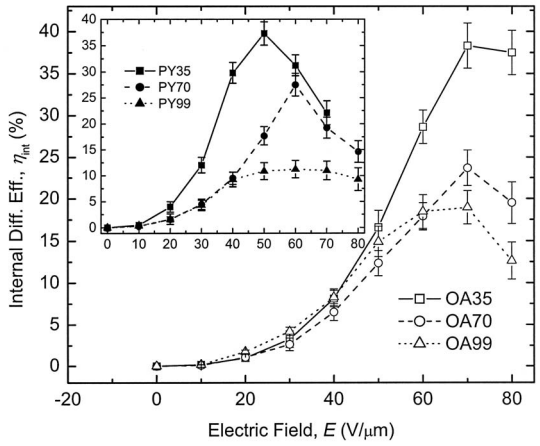

FIG. 6. Electric field dependence of the internal diffraction efficiencies η_{int} for the PR devices used in this study. The lines are guides for the eye.

obtained for the OA35 device and represents the maximum η_{int}, obtained for this series of devices. Assessment of the data reveals that as the concentration of NiS:OA is increased, the η_{int} decreases. As with the TBC gain coefficient, these results are contradictory to the expected outcome. It was anticipated that by increasing the concentration of the charge-generating species, an enhancement in the PR performance would ensue. In previous studies employing similar hybrid PR composites, the anticipated behavior was observed.[18] In this previous study CdTe was used as the charge-generating photosensitizer, and as its concentration was increased, an increase in η_{int} was observed. As with the TBC gain coefficient, this unexpected behavior is attributed to the fact that the NiS nanoparticles used in this study are not only acting as a charge-generating species but also as a charge-trapping component.

The η_{int} measured for the NiS:PY series of devices are presented in the inset of Fig. 6. This figure reveals that, as with the NiS:OA photosensitized devices, the device containing smallest concentration of photosensitizer, PY35, shows the greatest PR performance with $\eta_{int}=37.3\%$ at $E \approx 50$ Vμm. While this does not represent an increase in η_{int} relative to the OA35, the improved PR performance exhibited in the TBC experiment manifests itself as a significant lowering of the overmodulation field.

While the internal diffraction efficiencies are of fundamental importance, it is the external diffraction efficiencies η_{ext} which are of practical significance. The η_{ext}, accounting for reflections, was determined according to the equation

$$\eta_{ext} = \frac{I_s}{I_p}, \tag{3}$$

where I_p is the intensity of the probe beam before the device and I_s is the intensity of the diffracted portion of the probe beam after the device. For the NiS:OA photosensitized devices, OA35 exhibited the greatest external diffraction efficiency with $\eta_{ext}=15.6\%$ at 70 V/μm, the overmodulation voltage. The remainder of the NiS:OA photosensitized devices exhibit a precipitous decrease in η_{ext} as the concentration of the NiS:OA photosensitizer is increased. This precipitous drop in η_{ext} can be attributed to a combination of the drop in the η_{int} in conjunction with the increase in absorption associated with the higher NiS:OA concentration. With regard to the NiS:PY photosensitized devices, the maximum η_{ext} measured was 14.6% at 50 V/μm for the PY35 device. As with the NiS:OA sensitized devices, as the concentration of the NiS:PY photosensitizer was increased, the η_{ext} exhibited a significant decrease in all measured voltages.

Also of practical importance is the response time of the PR composites. In this regard, the PR devices exhibited response times typical of other PVK-based composites. The response times of the PR devices used in this study were gauged in the DFWM experimental geometry by recording I_s as a function of time. Subsequently, the data were fitted to a biexponential function commonly employed in the analysis of dynamics of the index modulation buildup, yielding a fast time, t_f constant, as well as a slow time constant t_s.[25] With $E=70$ V/μm, $t_f=0.494\pm0.007$ s, and $t_s=17.5\pm0.2$ s for the PY35 device and $t_f=0.563\pm0.011$ s and $t_s=22.2\pm0.4$ s for the OA35 device. A slight decrease in t_f was observed as the nanocrystal concentration was increased for both series of devices.

The trap densities for the composites were qualitatively gauged by calculating the phase shift ϕ between the illumination pattern associated with the intersecting writing beams and the space-charge field. Here, it is assumed that a decrease in ϕ from the maximum possible value of 90° can be attributed to an increase in the trap density, which would prevent free charges, in the form of photogenerated holes, from migrating fully into the dark regions of the illumination pattern. Larger deviations from 90° being attributed to larger trap densities. In order to calculate the phase shift, the change in refractive index with respect to p-polarized probe beam used in the DFWM experiment Δn_p can be calculated using the equation[26]

$$\eta_{int} = \sin^2\left[\frac{2\pi\Delta n_p d}{\lambda(\cos\theta_1 + \cos\theta_2)}\right]. \tag{4}$$

The results of this manipulation were then employed in estimating ϕ according to the equation (neglecting any contribution from the diffusion field)[1,26,27]

$$\phi = \sin^{-1}\left(\frac{\Gamma\lambda}{2\pi\Delta n}\right) = \arctan\frac{E_g}{E_q}, \tag{5}$$

which are plotted as a function of E for the NiS:OA and the NiS:PY photosensitized devices in Fig. 7. The dependence of ϕ on N^* becomes apparent in recognizing that E_g is the component of E in the grating wave vector direction and E_q is the trap-limited saturation space-charge field, which is proportional to N^* as

$$E_q = \frac{eN^*}{\varepsilon_0\varepsilon_r\mathbf{K}_G}, \tag{6}$$

where ε_0 is the permittivity of free space, ε_r is the permittivity of the composite, $\mathbf{K}_G$ is the grating wave vector, and e is the fundamental unit charge.[1] In Fig. 7, it is immediately apparent that as the concentration of NiS:OA is increased, ϕ decreases. Since the NiS:OA concentration is the only variable with respect to the device compositions, it is reasonable

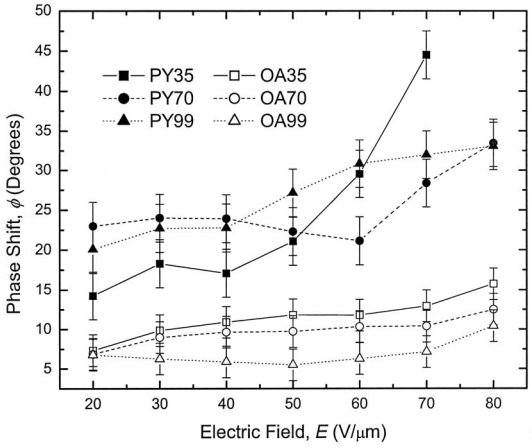

FIG. 7. Electric field dependence of the phase shift between the illumination pattern and the subsequent space-charge field ϕ for the PR devices used in this study. The lines are guides for the eye.

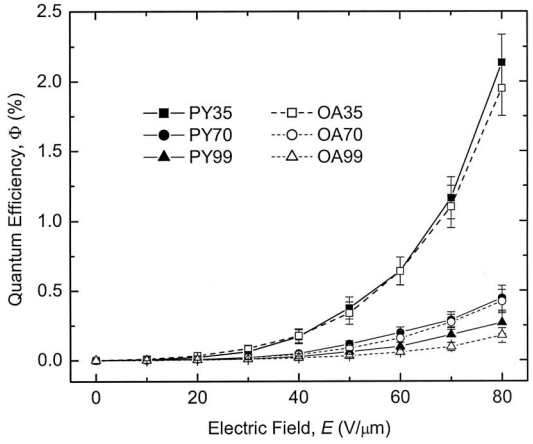

FIG. 8. Electric field dependence of the quantum efficiencies Φ of the PR devices used in this study. The lines are guides for the eye.

to conclude that the increase in the trap density is a direct consequence of the increasing concentration of NiS:OA, implying that the NiS:OA is acting not only as a charge-generating species but also as a trapping species as well. It is evident that ϕ for the NiS:PY photosensitized devices has increased relative to that of the NiS:OA photosensitized devices. Most likely, this is a result of the surface treatment imposed on the NiS:PY nanoparticles. Specifically, the number of surface defects, which are expected to act as trapping centers, has been reduced. Based on the reduced trapping potential of the NiS:PY, the concentration dependence of the observed ϕ is also reduced. For this reason, in conjunction with the indirect approach used in their calculation, the concentration dependence observed for the NiS:OA photosensitized devices is not as clearly evident for the NiS:PY photosensitized devices.

As described, an enhancement in the PR properties was anticipated as a result of the ligand exchange process, in which OA was replaced with pyridine as the passivating ligand. This speculation was based on the hypothesis that the conjugated nature of the pyridine molecule would be more conducive to the charge-transfer process than would be the relatively insulative OA molecule. In order to assess this premise, conductivity experiments were conducted, from which it was possible to directly determine the charge-generation quantum efficiencies Φ using the equation

$$\Phi = \frac{N_{cc}}{N_{ph}} = \frac{\sigma_p hcV}{I\lambda e\alpha d^2}, \tag{7}$$

where N_{cc} is the number of charge carriers generated per unit volume, N_{ph} is the number of photons absorbed per unit volume, h is Plank's constant, c is the speed of light, e is the fundamental unit charge, and V is the applied voltage. The Φ measured for the devices used in this study are depicted in Fig. 8. Evident in the figure is that for a given absorption (concentration of NiS), the Φ is slightly enhanced as a result of the ligand exchange. It was initially believed that this parameter could be improved as a result of enhanced charge transfer from the photosensitizing nanocrystal to that of the charge-transporting polymer. However, the evidence thus far suggests that this enhancement is more likely due to a decrease in the trapping centers associated with the surface modification. Also apparent from the figure is that for both NiS:OA and NiS:PY photosensitized PR devices, the Φ decreases as the concentration of nanocrystal is increased. This is in contrast to the expectation that Φ should be independent of concentration at low concentrations. This is further evidence that the increasing concentration of NiS:OA or NiS:PY increases the trap density within the material.

IV. SUMMARY AND CONCLUSION

In conclusion, although the anticipated benefit associated with substituting the OA passivating ligand for pyridine, specifically that of an enhancement in Φ, was not realized, an unexpected advantage was achieved. In particular, the charge-trapping characteristics of the photosensitizer were diminished. This modification ultimately resulted in a greater maximum Γ in the TBC experiment and led to a reduction in the overmodulation voltage in the DFWM experiment. The fact that the NiS:OA nanoparticles show a greater trapping tendency can be explained through the assumption that the ligand exchange process favorably modifies the surface of the nanoparticles by removing defects which can act as trapping centers. Also of significance is the fact that the NiS:PY photosensitized device exhibited a maximum diffraction efficiency of ~40%. This is the largest diffraction efficiency reported for a nanoparticle photosensitized device at this important wavelength.

ACKNOWLEDGMENTS

This work was supported by University of Missouri Research Board.

[1] *Photorefractive Materials and Their Applications*, Topics in Applied Physics I and II, edited by P. Gunter and J.-P. Huignard (Springer-Verlag, Berlin, 1988), Vols. 61–62.
[2] P. Yeh, *Introduction to Photorefractive Nonlinear Optics* (Wiley, New York, 1993).
[3] O. Ostroverkhova and W. E. Moerner, Chem. Rev. (Washington, D.C.) **104**, 3267 (2004).
[4] J. G. Winiarz and F. Ghebremichael, Opt. Express **12**, 2517 (2004).
[5] J. G. Winiarz and F. Ghebremichael, Appl. Opt. **43**, 3166 (2004).

[6] J. G. Winiarz, L. Zhang, M. Lal, C. S. Friend, and P. N. Prasad, Chem. Phys. **245**, 417 (1999).
[7] J. G. Winiarz, L. Zhang, M. Lal, C. S. Friend, and P. N. Prasad, J. Am. Chem. Soc. **121**, 5287 (1999).
[8] J. G. Winiarz, L. Zhang, J. Park, and P. N. Prasad, J. Phys. Chem. B **106**, 967 (2002).
[9] J. G. Winiarz and P. N. Prasad, Opt. Lett. **27**, 1330 (2002).
[10] D. J. Binks, S. P. Bant, D. P. West, P. O'Brien, and M. A. Malik, J. Mod. Opt. **50**, 299 (2003).
[11] K. R. Choudhury, J. G. Winiarz, M. Samoc, and P. N. Prasad, Appl. Phys. Lett. **82**, 406 (2003).
[12] C. Fuentes-Hernandez, D. J. Suh, B. Kippelen, and S. R. Marder, Appl. Phys. Lett. **85**, 534 (2004).
[13] F. Aslam, D. J. Binks, S. Daniels, N. Pickett, and P. O'Brien, Chem. Phys. **316**, 171 (2005).
[14] F. Aslam, D. J. Binks, M. D. Rahn, D. P. West, P. O'Brien, N. Pickett, and S. Daniels, J. Chem. Phys. **122**, 184713 (2005).
[15] K. R. Choudhury, Y. Sahoo, T. Y. Ohulchanskyy, and P. N. Prasad, Appl. Phys. Lett. **87**, 073110 (2005).
[16] K. R. Choudhury, Y. Sahoo, S. Jang, and P. N. Prasad, Adv. Funct. Mater. **15**, 1751 (2005).
[17] N. Cho, K. R. Choudhury, R. B. Thapa, Y. Sahoo, T. Ohulchanskyy, A. N. Cartwright, K.-S. Lee, and P. N. Prasad, Adv. Mater. (Weinheim, Ger.) **19**, 232 (2007).
[18] J. G. Winiarz, J. Phys. Chem. C **111**, 1904 (2007).
[19] Y. Xu and M. A. A. Schoonen, Am. Mineral. **85**, 543 (2000).
[20] A. Ghezelbash and B. A. Korgel, Langmuir **21**, 9451 (2005).
[21] M. A. Díaz-García, D. Wright, J. D. Casperson, B. Smith, E. Glazer, W. E. Moerner, L. I. Sukhomlinova, and R. J. Twieg, Chem. Mater. **11**, 1784 (1999).
[22] P. Magdolen, M. Mečiarová, and Š. Toma, Tetrahedron **57**, 4781 (2001).
[23] F. Aslam, J. Stevenson-Hill, D. J. Binks, S. Daniels, N. L. Pickett, and P. O'Brien, Chem. Phys. **334**, 45 (2007).
[24] W. E. Moerner and S. M. Silence, Chem. Rev. (Washington, D.C.) **94**, 127 (1994).
[25] M. Eralp, J. Thomas, G. Li, S. Tay, A. Schülzgen, R. A. Norwood, N. Peyghambarian, and M. Yamamoto, Opt. Lett. **31**, 1408 (2006).
[26] R. Bittner, K. Meerholz, G. Steckman, and D. Psaltis, Appl. Phys. Lett. **81**, 211 (2002).
[27] F. Wang, Z. Chen, B. Zhang, Q. Gonga, K. Wu, X. Wang, B. Zhang, and F. Tang, Appl. Phys. Lett. **75**, 3243 (1999).